

A hemocyanin-derived antimicrobial peptide from the penaeid shrimp adopts an alpha-helical structure that specifically permeabilizes fungal membranes

Petit Vanessa W.¹, Rolland Jean-Luc², Blond Alain¹, Cazevieille Chantal⁴, Djediat Chakib¹, Peduzzi Jean¹, Goulard Christophe¹, Bachère Evelyne², Dupont Joëlle³, Destoumieux-Garzón Delphine^{2,a}, Rebuffat Sylvie^{1,a}

¹ Laboratory Molécules de Communication et Adaptation des Microorganismes (MCAM, UMR, 7245), Muséum national d'Histoire naturelle (MNHN), Centre national de la Recherche scientifique (CNRS), Sorbonne Universités, 75005 Paris, France

² Interactions Hôtes-Pathogènes-Environnements (IHPE), Ifremer, CNRS, UPVD, Université de Montpellier, UMR, 5244, 34090 Montpellier, France

³ Institut de Systématique, Evolution, Biodiversité (ISYEB, UMR, 7205), MNHN, Université Pierre et Marie Curie (UPMC), CNRS, Sorbonne Universités, 75005 Paris, France

⁴ COMET, Plateau de microscopie électronique, Plateforme Montpellier RIO Imaging, 34091 Montpellier, France

^a Both authors have equally contributed to the present article.

* Corresponding author : Sylvie Rebuffat, email address : rebuffat@mnhn.fr

Abstract :

Background.

Hemocyanins are respiratory proteins with multiple functions. In diverse crustaceans hemocyanins can release histidine-rich antimicrobial peptides in response to microbial challenge. In penaeid shrimp, strictly antifungal peptides are released from the C-terminus of hemocyanins.

Methods. T

The three-dimensional structure of the antifungal peptide PvHCt from *Litopenaeus vannamei* was determined by NMR. Its mechanism of action against the shrimp pathogen *Fusarium oxysporum* was investigated using immunochemistry, fluorescence and transmission electron microscopy.

Results.

PvHCt folded into an amphipathic α -helix in membrane-mimicking media and displayed a random conformation in aqueous environment. In contact with *F. oxysporum*, PvHCt bound massively to the surface of fungal hyphae without being imported into the cytoplasm. At minimal inhibitory concentrations, PvHCt made the fungal membrane permeable to SYTOX-green and fluorescent dextran

beads of 4 kDa. Higher size beads could not enter the cytoplasm. Therefore, PvHCt likely creates local damages to the fungal membrane. While the fungal cell wall appeared preserved, gradual degeneration of the cytoplasm most often resulting in cell lysis was observed in fungal spores and hyphae. In the remaining fungal cells, PvHCt induced a protective response by formation of daughter hyphae.

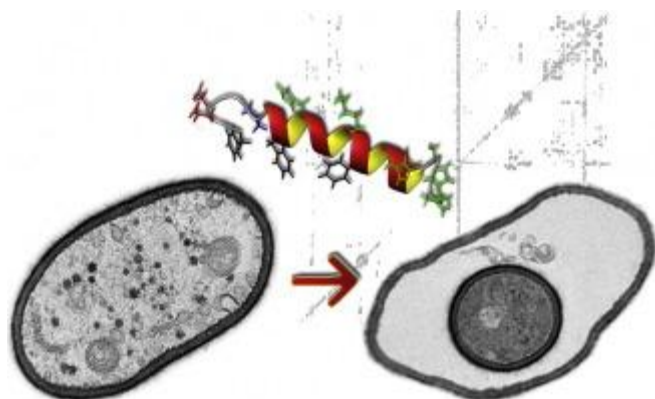
Conclusion.

The massive accumulation of PvHCt at the surface of fungal hyphae and subsequent insertion into the plasma membrane disrupt its integrity as a permeability barrier, leading to disruption of internal homeostasis and fungal death.

General significance.

The histidine-rich antimicrobial peptide PvHCt derived from shrimp hemocyanin is a strictly antifungal peptide, which adopts an amphipathic α -helical structure, and selectively binds to and permeabilizes fungal cells.

Graphical abstract



Highlights

► First description of a hemocyanin-derived antifungal peptide mechanism of action ► PvHCt is a histidine-rich antifungal peptide encrypted in shrimp hemocyanin ► The hemocyanin-derived antifungal peptide folds into an alpha-helix ► PvHCt binds to fungal cells and specifically permeabilizes fungal membranes ► Fungal cell death results from specific peptide-induced fungal membrane damages

Keywords : antimicrobial peptide, amphipathic helix, fungi, membrane bilayer, nuclear magnetic resonance (NMR), fluorescence microscopy

1. Introduction

Antimicrobial peptides (AMPs) have become recognized as important components of the innate immune system in a variety of organisms, ranging from plants to animals [1,2]. In invertebrates, which lack the so-called acquired immunity, the role of AMPs is believed to be even stronger. Most eukaryotic antimicrobial peptides are positively charged and contain hydrophobic amino acids. Although highly diverse in their primary structures, AMPs share a common feature of amphipathicity. Most cationic AMPs are membrane-active: they insert into and destabilize microbial membranes by pore formation or detergent effect [3]. Alternatively, AMPs can translocate across membranes and/or inhibit fundamental metabolic functions of microorganisms [4]. AMPs have been tentatively classified into three main classes according to their amino acid compositions and three-dimensional structures: (i) linear peptides tending to adopt α -helical amphipathic structures, (ii) peptides stabilized by disulfide bonds, which form β -sheet or mixed α -helix/ β -sheet structures, (iii) peptides with an over-representation of particular amino acids such as Arg, Gly, Pro or Trp, which adopt extended structures [1].

Major progress has been made over the past decade in the antimicrobial response of economically relevant species of marine molluscs and crustaceans [5,6]. In particular, due to their major production worldwide and to the huge economic losses caused by infectious diseases, penaeid shrimps have been the subject of a significant investigative effort. Viruses and to a lesser extent bacteria are the most serious shrimp pathogens [7,8], fungal diseases (mainly due to *Fusarium*) being less frequent, but severe and deleterious [9]. Several families of gene-encoded peptides displaying antifungal activities have been reported in shrimp, which could contribute to their innate capacity to fight fungal infections. Penaeidins, which have been identified in penaeid shrimp only, are both active against bacteria and filamentous fungi [10,11]. Their antifungal activity is believed to be mediated by their ability to bind chitin [12]. In addition to penaeidins, antilipopopolysaccharide factors (ALFs), which form a functionally divergent family of AMPs from crustaceans [13], are essential in shrimp defense against fungal, bacterial and viral infections [14,15]. The three-dimensional structures of both penaeidins and ALFs have been determined [16,17]. Finally, stylicins, which form a family of LPS-binding AMPs isolated from penaeid shrimp, were shown to display potent activities against filamentous fungi [18].

Beside gene-encoded AMPs, a 23 amino acid-antifungal peptide termed PvHCt (Fig. 1) was shown to participate to penaeid shrimp antimicrobial defense. PvHCt results from the proteolytic cleavage of the C-terminal end of the *Litopenaeus vannamei* hemocyanin, the major protein of shrimp plasma, in response to a microbial challenge [19]. PvHCt displays a high content in histidine (5 out of 23 residues), and also contains 3 anionic residues. Although most of the known eukaryotic AMPs are gene-encoded cationic peptides, there are now a substantial number of anionic AMPs, which like PvHCt are encrypted within the primary sequence of precursor proteins and released by proteolysis in response to infection [20]. PvHCt corresponds to the most acidic C-terminal sequence of *L. vannamei* hemocyanins (gene accession number AHY8647) (Fig.1). Generation of AMPs by cleavage of hemocyanin C-terminus was also described in the crayfish *Pacifastacus leniusculus*, with a 16 amino acid antibacterial peptide called astacidin-1 [21]. Contrary to astacidin-1, PvHCt from *L. vannamei* and the longer PsHCt-1 and -2 from *L. stylirostris* are antifungal but not antibacterial [19]. To our knowledge, this family of antifungal peptides is the only one to be characterized in penaeid shrimp species. PvHCt is the smallest antimicrobial peptide isolated from *L. vannamei* plasma. It has a broad spectrum of antifungal activity with minimum inhibitory concentrations (MICs) in the range 3-50 μ M. In particular, it inhibits the spore germination of the shrimp pathogen *Fusarium oxysporum* [19]. While the mechanisms underlying the antibacterial activity of AMPs have often been studied in details, much less attention has been paid to the mechanism of action of antifungal peptides from animal species. Most of the current knowledge comes from plant defensins, a family of cysteine-stabilized $\alpha\beta$ defensins that display a broad diversity of antifungal mechanisms of action [22].

Here we elucidated the mechanism underlying the strictly antifungal activity exerted by the shrimp hemocyanin-derived peptide PvHcT. By a combination of circular dichroism (CD) and ^1H NMR techniques, we showed that PvHcT is an amphipathic α -helical peptide that acquires its three-dimensional structure under membrane-mimicking conditions. We showed that PvHcT strongly binds to the surface of *F. oxysporum* hyphae and induces local membrane damages that result in cytoplasm gradual degeneration and fungal cell death.

2. Materials and methods

2.1. Materials

Egg phosphatidylcholine (PC), ergosterol, cholesterol and melittin from venom of the honey bee *Apis mellifera* were from Sigma-Aldrich (France). Carboxyfluorescein (CF) was from Eastman Kodak (France). All reagents used were of analytical grade.

2.2. Synthetic peptides

Synthetic peptides (purity > 98 %) either unprotected (PvHcT; MW = 2750 Da) or acetylated at the N-terminus and amidated at the C-terminus (Ace-PvHcT-NH₂; MW = 2791 Da) were purchased from Genecust and Genepep, respectively. Peptide purity and mass identity were assessed by matrix-assisted laser desorption/ionization time of flight mass spectrometry (MALDI-TOF). The spectra were recorded on an Applied Biosystems Voyager-DE-Pro instrument using α -cyano-4-hydroxycinnamic acid as the ionization matrix.

2.3. Microorganisms

Fusarium oxysporum (generous gift from Dr. Alain Vey, INRA, St. Christol-les-Alès, France), *Escherichia coli* (MCAM, MNHN Paris) and *Staphylococcus aureus* (IBMC Strasbourg) were used in the assays.

2.4. Circular dichroism

CD spectra were recorded on a Jasco J-810 instrument equipped with a Peltier effect-based thermostated cell holder. Samples were studied in quartz cells with path lengths of 0.5 mm at 25°C. Synthetic PvHcT and Ace-PvHcT-NH₂ were dissolved at 150 μM either in water at pH 5, in 10 mM phosphate and citrate buffer at pH 7 and pH 3, respectively or in methanol. Spectra were acquired in the absence or in the presence of 100 mM dodecylphosphocholine (DPC) micelles at both pH values and in the absence or presence of 100 mM sodium dodecyl sulphate (SDS) micelles at pH 7. The spectral contribution from the background was subtracted and the CD signals were normalized to the peptide concentration and expressed as the mean residue weight ellipticity values $[\theta]$ in $\text{deg.cm}^2.\text{dmol}^{-1}$. Samples were scanned over the 190-250 nm wavelength range by recording values every 1 nm with 50 nm min^{-1} scan rate, 1 s response time and 1 nm band width. Each spectrum was the average of 5 scans. Deconvolution of CD spectra was achieved using different deconvolution methods [23]; Dichroweb (<http://dichroweb.cryst.bbk.ac.uk/html/home.shtml>).

2.5. NMR spectroscopy

NMR data were acquired on a 400 MHz AVANCE 400 spectrometer equipped with a $^1\text{H}/\text{X}$ Z-gradient BBI probehead and BCU-05 refrigeration / BVT 3000 temperature control unit and a 600 MHz AVANCE III HD 600 spectrometer equipped with a triple resonance $^1\text{H}-^{13}\text{C}-^{15}\text{N}$ TCI cryoprobe with Z-gradient (Bruker Biospin, Wissembourg, France). Synthetic unprotected PvHcT and modified Ace-PvHcT-NH₂ peptides were dissolved in H₂O/D₂O (90:10) at pH 3.5 in the absence or presence of 350 mM *d*₃₈-DPC and in *d*₃-methanol (CD₃OH), respectively to yield NMR samples of final 3.5 mM peptide concentration. A 100 fold molar excess of DPC was used to minimize the possibility of peptide/peptide interactions. ^1H chemical shifts were referenced to 2,2-dimethyl-2-silapentane-5-sulfonate (DSS) at 0.00 ppm for experiments in H₂O/D₂O and in DPC micelles, or to the central component of the quintet due to the CD₂HOH resonance of methanol taken at 3.313 ppm, downfield

from TMS. For sequential assignments and structure determination, recorded data sets included COSY, TOCSY with a MLEV spin lock of 100 ms, NOESY, with 100, 200 or 400 ms mixing times, within the temperature range of 288-323 K to identify overlapping spin systems. Solvent signal suppression was achieved by using the pulsed-field gradient-based Watergate method in the pulse sequences at 400 MHz or fulfilled by using excitation sculpting (600 MHz). Data were collected and processed using Bruker XWIN-NMR, AURELIA and TOPSPIN 3.2 softwares (Bruker Biospin, Wissembourg, France).

2.6. Structure determination

The cross peak volumes of the 200 ms NOESY spectra were measured, calibrated with respect to the cross-peak volume of the Pro5 geminal β -protons, which correspond to an interproton distance of 1.8 Å, and converted into distance constraints using AURELIA software. When no stereospecific assignments could be made for the methyl and methylene protons, appropriate pseudoatom corrections were applied [24] and lower distance bounds were taken as the sum of the van der Waals radii of 1.8 Å. A total of 215 and 134 upper and lower distance constraints were used for structure calculations of PvHct and Ace-PvHct-NH₂ in DPC micelles and CD₃OH, respectively. For calculation of the solution structure of Ace-PvHct-NH₂ in CD₃OH, eight Φ dihedral angles, inferred from the $^3J_{\text{HNC}\alpha\text{H}}$ coupling constants measured from the 1D spectrum taken at 303 K were taken into account and restrained to $-60 \pm 30^\circ$ for a $^3J_{\text{HNC}\alpha\text{H}}$ lower than 6 Hz (Gly8, His9, Ile10, Lys13, Val14, Phe15, His17 and Gly18). The three-dimensional structures of PvHct and Ace-PvHct-NH₂ compatible with the experimental distance restraints obtained in DPC micelles and in CD₃OH, respectively were calculated using a standard simulated annealing protocol with the program X-PLOR [25], with a target function similar to that used by Nilges *et al.* [26]. An *ab initio* simulated annealing protocol [26] was used to generate a first set of 100 structures, starting from a template structure with randomised Φ , ψ angles and extended side chains and only taking into account the intraresidue, sequential, medium- and long-range restraints. For the Ace-PvHct-NH₂ structure in methanol solution, the NOE restraints were checked for violations and further 100 structure sets were calculated with the inclusion of the 8 selected Φ dihedral angle restraints. Refinement of the structures was achieved using the conjugate gradient Powell algorithm of energy minimization, using the CHARMM22 force field (files topallh22x.pro and parallh22x.pro) [27]. Structures were visualized using MOLMOL [28] and analyzed with MOLMOL and PROCHECK-NMR [29]. The 20 best structures on the basis of their total energy including the electrostatic term, with no systematic NOE-derived distance violation larger than 0.2 Å for both PvHct and Ace-PvHct-NH₂ and no dihedral angle violation greater than 5° for Ace-PvHct-NH₂ were selected as the final structures of PvHct and Ace-PvHct-NH₂ in DPC micelles and CD₃OH solution. They showed no ideal geometry violation (RMSD <0.01 Å and $<2.2^\circ$ for bond lengths and valence angles, respectively).

The coordinates and NMR chemical shifts have been deposited in the Protein Data Bank and the Biological Magnetic Resonance Bank databases (accession numbers: PvHct: PDB 2N1C, BMRB 25555; Ace-PvHct-NH₂: PDB 2N30, BMRB 25631).

2.7. Spore germination and hyphal growth assays

F. oxysporum was grown at 25°C for 2 weeks on potato dextrose (Difco) agar medium. The spores were collected from the plates with sterile water, passed through a glass wool filter to remove hyphae and counted. For antifungal assays, fresh fungal spores were adjusted to 10^4 spores/ml in half-strength potato dextrose broth ($\frac{1}{2}$ PDB, Difco) at pH 5. Inhibition of spore germination was monitored in 96-well microplates, as described previously [19]. Briefly, each well received 80 μl of fungal spore suspension (10^4 spores/ml), 10 μl PvHct (serial dilutions ranging from 6 to 400 μM final concentration) and 10 μl sterile water. Growth controls contained 80 μl of fungal spores and 20 μl of sterile water. Spore germination was monitored under a light microscope after 24 h of incubation at 30°C in the dark. The ability of PvHct to inhibit hyphal growth was monitored by adding 10 μl of PvHct solution (final concentrations in the range of 6-400 μM) or of sterile water (control) to the spores (80 μl adjusted to 10^4 spores/ml) incubated for 13 h at 30°C in the presence of 10 μl sterile water. Growth inhibition was observed under a light microscope after 48 h of incubation at 30°C. The minimum inhibitory concentration (MIC) was defined as the lower peptide concentration at which the fungus did not exhibit visible growth.

2.8. SYTOX green uptake assay

The SYTOX green (Invitrogen-Molecular Probes) uptake assay was performed as described by Thevissen *et al.* [30]. *F. oxysporum* spores (10^4 spores/ml) were grown for 48 h at 30°C in 96-well microplates containing 150 μ l of ½ PDB medium (pH 5) until a mycelium covered the surface of microplate wells. In other microplate wells, 10^4 spores/ml were dispensed immediately before PvHCt-treatment. 15 μ l PvHCt (1.25-20 μ M final concentration) or an equal volume of water (control) were added to wells containing either hyphae or spores together with 0.5 μ M SYTOX green to monitor permeabilization of hyphae and spores. For bacterial cells, 150 μ L of *E. coli* B and *S. aureus* were grown at 37°C in Luria-Bertani (LB, pH 7.2) medium and adjusted to an absorbance at 620 nm of 0.3 before being incubated with 15 μ L PvHCt (1.25-20 μ M final concentration) and 0.5 μ M SYTOX green. SYTOX green uptake was monitored (λ_{ex} 480 nm / λ_{em} 550 nm) every 15 min over 2.5 h using a TECAN microplate reader. For microscopic observation of SYTOX green uptake, fungal and bacterial cells were treated as above for 2 h with PvHCt. Mellitin was used as a positive control. Excess peptides (PvHCt or mellitin) were removed by two washes in culture medium, before 0.5 μ M SYTOX green was added. Cells were visualized using an Olympus ix70 inverted fluorescence microscope equipped with standard green 495 nm-519 nm filter. Images were acquired with an Amotacam pro 282B camera (Motic).

2.9. FITC-dextran assay

The method described by Van der Weerden [31] was used with slight modifications. Briefly, hyphae were grown as above and incubated with PvHCt (1.25-50 μ M) or an equal volume of water for 2 h at room temperature in ½ PDB (pH 5). Hyphae were washed twice for 10 min with ½ PDB to remove PvHCt before 4 kDa- or 10 kDa-FITC-dextran (Sigma) were added to a final concentration of 1 mg/ml. Hyphae were incubated for 30 min at room temperature and then washed twice with ½ PDB to remove excess FITC-dextran. Hyphae were visualized as above using an Olympus ix70 inverted fluorescence microscope.

2.10. Liposome permeabilization assay

Carboxyfluorescein (CF)-loaded small unilamellar vesicles (SUV) were used to measure the PvHCt-induced permeabilization of liposomes, as described previously [32]. Briefly CF-entrapped SUVs were prepared by sonication (Heat Systems Ultrasonics model W-225R sonifier equipped with a microtip probe) of an egg phosphatidyl choline / ergosterol 7/3 mixture in Hepes buffer at pH 7.4. The CF-loaded SUVs were separated from unencapsulated CF by gel filtration over Sephadex G75. The peptide-induced release of CF at 20 min from the liposomes was measured as a percentage of the maximal fluorescence intensity obtained after total lysis of the liposomes by 0.5% Triton X100, and with a constant lipid concentration of 0.6 mM. CF fluorescence was monitored at 20°C on a Kontron SFM 25 spectrofluorometer, at excitation and emission wavelengths of 488 and 520 nm, respectively. The efficiency of the peptides tested was quantified by the $R_i^{-1} = [\text{peptide}] / [\text{lipid}]$ ratios. Melittin was used as positive control.

2.11. PvHCt immunostaining

To monitor PvHCt localization in *F. oxysporum*, hyphae were incubated in ½ PDB (pH 5) with PvHCt (400 μ M) or an equal volume of water for 2 h at room temperature. Hyphae were washed twice for 10 min with ½ PDB to remove PvHCt before immunostaining. Analyses were carried out using PvHCt polyclonal antibodies (lab product) as described in [33]. Briefly, after permeabilization with 0.1% Triton X-100 for 1 h, the hyphae were incubated overnight at 4°C with anti-PvHCt (4 μ g/ml) in PBS/Bovine Serum Albumine (PBS/BSA) at 0.5% or in PBS/BSA (control). After three washes in phosphate buffer saline (PBS) a second incubation was performed for 1 h at room temperature with anti-rabbit Alexa green 488-conjugated (Pierce) diluted at 1:400 in PBS/BSA 0.5%. After three washes in PBS, DAPI was added to the fixed tissues in the dark for 10 min. Upon staining, the fluorescent products generated by the two dyes were visualized using a wide-field Olympus ix70 inverted fluorescence microscope equipped with standard green (495 nm-519 nm, Alexa green 488)

and blue (358 nm-461 nm, DAPI) filters set and memorized using an Amotacam pro 282B camera (Motic).

2.12. Transmission electron microscopy

Hyphae – A 48h culture of *F. oxysporum* hyphae obtained as in the Sytox green uptake assay was exposed for 24 h at 30°C to 50 μ M PvHcT or an equivalent volume of sterile water (control) diluted in 1/2 PDB (pH 5). Hyphae were then fixed in 2.5% glutaraldehyde in PHEM buffer (1X, pH 7.4) overnight at 4°C. They were then rinsed in PHEM buffer and post-fixed in a 0.5% osmic acid for 2 h at dark and room temperature. After two rinses in PHEM buffer, the cells were dehydrated in a graded series of ethanol solutions (30-100%). The cells were embedded in EmBed 812 using an Automated Microwave Tissue Processor for Electronic Microscopy, Leica EM AMW. Thin sections (70 nm; Leica-Reichert Ultracut E) were collected at different levels of each block. These sections were counterstained with uranyl acetate and lead citrate and observed using a Tecnai F20 transmission electron microscope at 200KV at the CoMET MRI facilities, INM France.

Spores - *F. oxysporum* spores were adjusted to 10⁵ spores/ml in 1/2 PDB (pH 5) and exposed for 12 h at 30°C to PvHcT (750 μ M) or to an equal volume of sterile water (control). After two washes in 100 mM phosphate buffer, pH 7.4, spores were fixed for 3h at room temperature in 2 % glutaraldehyde diluted in the same buffer. Spores were then post-fixed with 1 % osmium tetroxide for 30 min at room temperature. After three washes in phosphate buffer, samples were dehydrated in a graded ethanol series (50-100 %) and embedded in low viscosity Spurr's medium (EMS: Electron Microscopy Science). Ultra-thin sections, 60-70 nm thick, were cut with a diamond knife and collected on Formvar-coated copper grids (EMS). Sections were stained with 2 % uranyl acetate in ethanol 50 % during 10 min, before examination under a Hitachi 7100 transmission electron microscope operated at 75 kV at the MNHN electron microscopy facilities.

3. Results

3.1. PvHcT adopts a helical conformation in membrane-mimicking media

The structure of PvHcT, the 23 residue C-terminal peptide resulting from cleavage of the shrimp *L. vannamei* hemocyanin, was studied using two synthetic peptides, PvHcT and Ace-PvHcT-NH₂. PvHcT is a free N- and C-terminus peptide devoid of posttranslational modification, which is identical to the original natural peptide and was used previously for the initial study of its spectrum of activity [19]. Ace-PvHcT-NH₂ is the N-acetylated and C-amidated analogue of PvHcT, which was used here to examine the effects of the N- and C-terminal charges on the peptide structure and activity. CD spectroscopy was used for secondary structure determination. In all the conditions tested, both PvHcT and Ace-PvHcT-NH₂ displayed very similar CD spectra, indicating that the charges at the peptide extremities have no effect on its global conformation. In phosphate buffer (pH 7) and citrate buffer (pH 3), the CD spectra of both peptides displayed a negative band at 200 nm characteristic of a random coil conformation (Fig. 2). Therefore, both PvHcT and its N-acetylated and C-amidated variant are unstructured in aqueous environments. In the presence of SDS micelles, the surface of which is anionic, the spectrum appeared modified but kept characteristics of a random coil conformation (Fig. 2A). On the contrary, in the presence of DPC micelles, which provide a lipid surface used to mimic phospholipid bilayer environments containing a high amount of zwitterionic phospholipids [34], such as fungal membranes [35], the spectrum displayed strong negative bands at 207 and 225 nm together with a strong positive band around 190 nm, indicating clearly a right-handed helical structure at both pH 7 (Fig. 2) and pH 3 (data not shown). A similar helical structure was observed for the N-acetylated and C-amidated Ace-PvHcT-NH₂ studied in an organic solvent like methanol, which provides an uncharged non-micellar amphipathic environment that coarsely mimics membranes (Fig. 2). Using different deconvolution methods, PvHcT was estimated to contain about 30-35% of helix and β -turns in these two environments and at both neutral and acidic pH. Whereas the hydrophobic/amphipathic environment was important for the peptide structuration, the pH and the N- and C-terminal charges of the peptide were not.

3.2. PvHCt adopts an amphipathic α -helical structure in membrane mimicking media

In agreement with our CD data (Fig. 2), the 1D proton, TOCSY and DQF-COSY NMR spectra of PvHCt in aqueous media showed a random-coil conformation for the peptide (Figs S1-S6). The spectra in water indeed displayed little resonance dispersion in the NH and H α regions and the $^3J_{\text{HNC}\alpha\text{H}}$ coupling constants were around 7 Hz. The solution structures of PvHCt and Ace-PvHCt-NH₂ were then analysed in DPC micelles and in methanol (Figs. S7-S15), in which PvHCt was well structured as determined by CD spectroscopy (Fig. 2). Despite several identical amino acids in the sequence, in particular the 5 histidines, identification of all spin systems was achieved in both media from the analysis of COSY, TOCSY, and NOESY spectra (Figs S8 and S12). As for the proline at position 5, the presence of NOE cross peaks involving the Pro5 H δ and the Leu4 H α was indicative of a *trans* conformation of the peptide bond in both environments. The chemical shift indexes (CSI) determined for the α -protons with respect to random coil statistical values [36] showed mainly negative deviations indicative of a helical structure in the central region (residues 6-20) (Fig. S15). The presence of strong $d\alpha\beta(i, i+3)$ and $d\alpha N(i, i+3)$, together with numerous successive $dNN(i, i+1)$, as well as of several $d\alpha N(i, i+2)$ and/or $d\alpha N(i, i+4)$ occurring without interruption from residue 6 to 19 in the NOESY spectra taken in DPC micelles and in methanol (Fig. S15), also indicated that PvHCt forms a continuous α -helix in the central region in these two environments. The $^3J_{\text{HNC}\alpha\text{H}}$ coupling constants < 6 Hz measured in methanol for Gly8, His9, Ile10, Lys13, Val14, Phe15, His17 and Gly18 were in agreement with the helical structure (Fig. S15). We observed that the α -helix starts after the Pro5 residue known to initiate helices [37,38].

The final sets of conformers calculated for PvHCt and Ace-PvHCt-NH₂ in DPC micelles and in methanol, respectively (Fig. 3) showed that both peptides adopt α -helical structures encompassing the central region (residues 6-16 in DPC micelles, 8-18 in methanol). The remaining N- and C-terminal extremities were disordered. The structural statistics are summarized in Table 1. In 10 % of the structures calculated for the DPC micelle environment, the helix contains 3₁₀ helix parts, while it is only of the α -type in methanol. The side-chain orientations indicate that PvHCt and Ace-PvHCt-NH₂ helices have a marked amphipathic character due to well-defined aromatic and potentially basic sectors (Fig. 3B, C, E, F). The basic residues (Lys, His) are lining up on one face of the helix, while the aromatic residues (Phe) form a hydrophobic sector on the other side. Finally, depending on the pH, the N- and C-terminal regions can be negatively and positively charged respectively, due to the localization of Glu2, Asp3 at the N-terminus and of His22, His24 at the C-terminus. As a result, PvHCt adopts an amphipathic α -helical structure in membrane-mimicking environments and belongs to the class of the α -helical antimicrobial peptides

3.3. PvHCt does not permeabilize egg PC/ergosterol liposomes

PvHCt and Ace-PvHCt-NH₂ were observed in our assays to have similar activity on *F. oxysporum* spore germination with MIC of 12.5 μM , as previously described [19], and on hyphal growth. To determine if this antifungal activity involves a specific interaction with major membrane components, we examined whether PvHCt could induce membrane damages in artificial membranes composed of a zwitterionic phospholipid (phosphatidylcholine, PC) and ergosterol, the sterol specific to fungal membranes. Small unilamellar vesicles (SUVs) of PC/ergosterol 7:3 were loaded with carboxyfluorescein (CF, molecular mass \sim 0.37 kDa) and the CF leakage was monitored by fluorescence spectroscopy. Even at high R_i^{-1} peptide to lipid ratios up to 50×10^{-3} , which corresponds to 1 peptide molecule for 20 lipids, PvHCt was unable to induce any CF leakage (data not shown). By contrast melittin, which is known to exert its antifungal activity by membrane permeabilization and lysis [39], induced 100 % CF leakage at the much lower peptide to lipid ratio of 5×10^{-3} (1 peptide for 200 lipids).

3.4. PvHCt binds to the surface of fungal cells

To localize PvHCt on *F. oxysporum* cells, hyphae were treated with 400 μM PvHCt (20 times the MIC) before immunostaining with anti-PvHCt polyclonal antibodies. An intense green fluorescence indicative of PvHCt binding was observed at the surface of PvHCt-treated hyphae, which was not visible in non-treated controls (Fig. 4). Despite the high concentration of PvHCt used, the hyphae

intracellular space was negative to antibody staining, indicating that PvHCt most likely stays at the fungal wall and/or at the membrane (Fig. 4).

3.5. PvHCt compromises fungal but not bacterial membrane integrity

We examined the membrane-activity of PvHCt on live cells by treating fungal and bacterial cells with PvHCt (10, 20 μ M) and monitoring the uptake of SYTOX Green, a fluorescent dye that intercalates into the DNA strands of cells having a damaged plasma membrane. *F. oxysporum* hyphae were observed by epifluorescence microscopy. At 10 μ M, all the hyphae were not stained by SYTOX green, while at 20 μ M, *i.e.* above the MIC (12.5 μ M), all hyphae were stained (Fig. 5A). Similarly, spores of *F. oxysporum* treated with PvHCt were positive to SYTOX Green staining (Fig S16). SYTOX Green uptake was then measured over a range of PvHCt concentrations. Fluorescence was detected even at the lowest PvHCt concentration (1.25 μ M) and increased in a dose-dependent manner to reach a threshold at 10 μ M PvHCt, which is close to the MIC. Fluorescence increased rapidly, being detected as soon as PvHCt was added to the *F. oxysporum* hyphae (Fig. 5B). Interestingly, neither *E. coli* B (Gram-negative) nor *S. aureus* (Gram-positive), which are not susceptible to PvHCt antimicrobial activity, could be stained by SYTOX green at 200 μ M peptide concentration (data not shown). In similar conditions, melittin used as a positive control was able to induce uptake of SYTOX green in *F. oxysporum*, *E. coli* and *S. aureus* (data not shown). From our data, PvHCt induces a selective and dose-dependent permeabilization of the hyphae of *F. oxysporum*, which is consistent with the MICs against this shrimp pathogen (Fig. 5B).

3.6. PvHCt causes local damages to the fungal membrane

To characterize the membrane damages caused by PvHCt in *F. oxysporum*, hyphae treated with increasing concentrations of PvHCt (10-50 μ M) were incubated with SYTOX green or FITC-labeled dextrans of two sizes, either 4 or 10 kDa. Dextrans of 4 kDa entered hyphae at the same PvHCt concentration that led to SYTOX green uptake (molecular mass \sim 0.65 kDa), whereas 10 kDa dextrans were excluded even at high PvHCt concentration (Fig. 6), suggesting damages of limited size were created in the membrane. To examine the stability of PvHCt-induced membrane damages, a second experiment was done in which SYTOX green and dextrans were added after removal of PvHCt by extensive washing. Both SYTOX green and 4 kDa FITC-dextran entered the hyphae after peptide washing (data not shown), indicating the persistence of the observed PvHCt-induced membrane damages.

3.7. PvHCt induces severe damages to *F. oxysporum* hyphae and triggers daughter hyphae formation

To get deeper insight into PvHCt mechanism of action, ultrastructural effects of the AMP on fungal spores were examined by transmission electron microscopy (TEM). Major ultrastructural changes were observed on PvHCt-treated hyphae. In particular, a large number of ghost cells were observed in which only cell walls remained visible (Fig. 7A). When the cytoplasmic material was still visible inside cells, most often the ultrastructure of the cell was completely disorganised, with a lack of intact organelles (Fig 7C-D). Remarkably, we observed a high number of cells containing daughter hyphae (Fig. 7A-C): hyphae appeared duplicated, a new hyphae being surrounded by the cell wall, and occasionally the cytoplasmic content of the parent hyphae. Most of the time, the parent hyphae had lost its integrity. Common observations were a loss and/or condensation of the cytoplasmic content (Fig 7C-D), and cell wall disruption of the parent hyphae (Fig 7A). Daughter hyphae often showed a preserved ultrastructure (Fig 7B). In some cases, both the parent and the daughter hyphae were disrupted. Non-treated hyphae (controls) showed a preserved ultrastructure and a total absence of daughter hyphae formation (Fig 7E-F).

3.8. PvHCt disrupts the ultrastructure of fungal spores and blocks the spore metabolism

We also observed major ultrastructural changes induced by PvHCt on fungal spores. Before the beginning of germination (t_0), all untreated spores displayed plasma membranes surrounded by very clear cell walls. The control spores showed a large content in lipid bodies (Fig. 8A), 77 % of the spores presenting such structures (Table 2). Numerous mitochondria were observed, while peroxisomes were completely absent at t_0 (Table 2). After a 12 h-incubation at 30°C (t_{12}), 63% of the

control spores showed the development of electron-dense peroxisomes (Fig. 8B), while a decrease in the number of lipid bodies was observed (from 77% to 37% of the spores) (Table 2). Both events are associated with the beginning of spore germination. No mitochondria were observed. In PvHCt-treated *F. oxysporum* spores fixed 12 h after treatment (t12PvHCt), highly damaged ultrastructures were observed (Fig. 8C). As in t12 controls, the number of spores containing lipid bodies was reduced down to 43%. However, contrasting with the t12 controls, PvHCt induced a major disorganization of the cytoplasm, with a damaged plasma membrane (Fig. 8C) and a large number of cell debris (observed in 40% of the spores). Few mitochondria remained observable. Finally, PvHCt-treated spores showed a total absence of peroxisomes, which indicated an arrest of the metabolic activity.

4. Discussion

We characterized here the three-dimensional structure and antifungal mechanism of action of PvHCt, a hemocyanin-derived antifungal peptide released in shrimp plasma in response to infection. Results from the present article showed that PvHCt adopts an α -helical structure in membrane-mimicking media and specifically inserts into fungal membranes thereby creating severe damages to fungal spores and hyphae leading to cytoplasm degeneration and ultimately cell death.

4.1. Structure of PvHCt

PvHCt was shown to adopt an amphipathic α -helical structure in membrane-mimicking environment, while it was unstructured in aqueous medium (Figs 2-3). Similarly, a number of AMPs adopt an active amphipathic α -helical structure upon interaction with membranes or micelles. Like PvHCt, which contains 5 histidines out of 23 residues (22%), several α -helical AMPs are histidine-rich peptides. Indeed, moronecidin / piscidin [40,41], clavansins [42] and histatin 5 [43,44], which are highly cationic AMPs, contain 4 to 7 histidines out of 22 to 24 residues (18 to 29 %) and adopt helical structures. α -helical antibacterial peptides often carry N-terminal helices stretching from the very first residues [45,46,47,48]. In many cases the helices contain a bend, which is generally due to the presence of proline or glycine, two residues known to generate flexibility and induce kinks in helices, due to the absence of an amide proton and of a side chain on the α -carbon, respectively. On the contrary, in the antifungal peptide PvHCt, we found that the helix spans the central part of the sequence and starts after Pro5 in methanol solution or at Gly8 in DPC micelles (Fig 3). These residues could act as flexible hinges in PvHCt, thus facilitating a deeper membrane insertion, as observed for other AMPs [49,50]. The N- and C-terminal extremities remain unordered, affording presumably two more flexible short regions. The helix encompasses two well-defined sectors with different charge and polarity, thus exhibiting a clear amphipathic character. A hydrophobic face assembles the most hydrophobic and aromatic residues, while charged and more polar residues are lining on a polar face (Fig. 3). The N- and C-terminal extended extremities bear a negatively-charged and a positively-charged patch, respectively. This amphipathic helical structure likely contributes to the interaction of PvHCt with the fungal plasma membrane: two phenylalanines included in the helical region (Phe7, Phe15) could indeed participate in the interaction with the membrane bilayer and be preferentially located at the bilayer interface, as demonstrated for LL-37 or clavansin [50,51]. The aromatic imidazole groups of the histidines, which are only partially protonated at pH values around 6.5, could also contribute to the interaction. Altogether, our NMR and CD results indicate PvHCt has the potential to form an amphipathic α -helix in contact with biological membranes and to further interact with phospholipid bilayers by the anchoring of phenylalanine and histidine residues and the flexibility arising from Pro5 and Gly8.

4.2. Binding of PvHCt to the fungal cell surface

PvHCt was found to bind massively to the cell surface of *F. oxysporum* but not to enter into the hyphae cytoplasmic space. Indeed, a strong fluorescent labelling of the surface of hyphae was observed upon immunostaining with anti-PvHCt antibodies, but the hyphae intracellular space remained free of labelling (Fig. 4). Therefore, the fungal cell wall and/or membrane appear to be important cellular targets for PvHCt. The essential role of fungal cell wall components in initiating the insertion of strictly antifungal peptides into fungal membranes has been previously reported for the

histidine-rich histatin-5 [52] and NaD-1 defensin [53]. We observed in this study a damaging interaction of PvHCt with fungal but not bacterial membranes (Figs 5-6). Binding of AMPs to biological membranes is often driven by electrostatic interactions between the negatively charged membranes of fungi and bacteria and the positive charges of cationic AMPs [3]. However, PvHCt displays a theoretical pI of 6.16 (Fig.1). Although this is rather unusual among AMPs including the histidine-rich AMPs previously mentioned, an increasing number of anionic AMPs have now been described with net negative charges in the range of -3 to -2 at physiological pH [20]. PvHCt contains three negatively charged amino acids. Importantly, it also contains 5 histidines that behave as cationic residues at pH values below 6 and as aromatic uncharged residues at pH 6-7. As a consequence, PvHCt net charge can rapidly revert from -2 to +3 in a narrow range of pH values close to the physiological pH inside spores and hyphae (pH 6.5-7.0) [54]. Similarly, PvHCt is expected to behave as a cationic peptide at the pH of antifungal assays (pH 5) but as an anionic peptide at the pH of antibacterial assays (pH 7.2). This may have important consequences on electrostatic interactions between PvHCt and biological membranes and consequently on the selectivity of PvHCt towards fungi. However, from our CD and NMR data, PvHCt adopts an amphipathic α -helical structure in zwitterionic membrane mimicking media at both pH 3 and 7 (Figs 2-3). Moreover, the additional charges at the two extremities of the peptide were found here not to be critical, neither for the structure acquisition nor for the antifungal activity. Altogether, those results suggest that hydrophobicity is a stronger driver than charge in the interaction of PvHCt with biological membranes.

4.3. PvHCt creates damages to the fungal membrane

PvHCt was shown to create local damages to the membrane of the shrimp pathogen *F. oxysporum*. First, we found that PvHCt induced a massive uptake of SYTOX green in *F. oxysporum* spores and hyphae, which cannot cross the membrane of live cells, but readily penetrates compromised plasma membranes. From our results, the plasma membrane of *F. oxysporum* spores and hyphae is rapidly compromised (within a few minutes) upon incubation with PvHCt (Fig. 5). The level of damages induced by PvHCt on *F. oxysporum* hyphae was shown to be dose-dependent, the maximum of SYTOX green fluorescence being observed between 10 and 20 μ M (Fig. 5), which correlates with the minimal inhibitory concentrations (MIC 12.5 μ M).

In addition, at concentrations close to the MIC, the membrane damages were found to be limited in size. Indeed, FITC-dextran beads with a size of 10 kDa (average globular diameter 23 Å) were unable to reach the cytoplasm of PvHCt-treated samples unlike 4 kDa beads (average globular diameter 14 Å) (Fig. 6). Similar observation of FITC-dextran selective uptake were interpreted as indicative of pore formation in filamentous fungi treated with the NaD1 plant defensin [31]. However, unlike PvHCt, the cationic antifungal defensin NaD1 massively enters the cytoplasm of filamentous fungi, in a process that requires the Agp2p membrane protein and likely relies on electrostatic interactions between NaD1 and the membrane [55]. Formation of pores has also been proposed for astacidin-1, a 16-mer antibacterial peptide (theoretical pI=10), which contains two putative β -sheets [21], and was recently found to depolarize the membrane of yeast cells [56].

Although in depth studies would be required to determine the precise nature of the peptide/membrane interactions [57], the three-dimensional structure of PvHCt is consistent with the capacity of PvHCt to insert into biological membranes as demonstrated in our fungal membrane permeabilization assays. Indeed, the amphipathic character of α -helical peptides is recognized as a major determinant of the capacity of hydrophobic and cationic AMPs to insert into membrane bilayers [3] [58]. This is now also recognized for membrane-active anionic AMPs [20]. Thus, targeting of the fungal plasma membrane has arisen as a convergent mechanism of action among antifungal peptides of diverse charges and three-dimensional structures.

4.4. Final stage of fungal killing by PvHCt

Besides inhibiting spore germination, we showed here that PvHCt prevents hyphal growth. In our TEM observations, PvHCt created severe damages to the hyphae structures with a gradual degeneration of the cytoplasm, which often resulted in cell lysis, as indicated by abundant ghost cells, disrupted membranes and occasionally disrupted cell walls. Most of the remaining live fungal cells gave birth to daughter hyphae by producing new wall material inside the original hyphal cells, a protective response also reported in filamentous fungi exposed to a fungicide treatment like

tebuconazole [59]. Many of the original hyphae appeared collapsed and in some rare cases, the daughter hyphae appeared to grow out of the original hyphae (Fig. 7).

TEM experiments on *F. oxysporum* spores allowed to get insight into the ultimate state of *F. oxysporum* killing by PvHcT. As with hyphae, PvHcT induced major cytoplasmic and plasma membrane damages in spores (Fig. 8). The PvHcT-mediated arrest of growth was associated with the absence of peroxisomes, which were conversely observed in most of the germinating spore sections (controls). Among the functions of peroxisomes are the sequestration of oxidative steps in lipid metabolism including β -oxidation of fatty acids, and steps in the synthesis of sterols, isoprenoids, ether-phospholipids, and polyunsaturated fatty acids [60]. The absence of this organelle in the PvHcT-treated spores is not only consistent with the observed growth arrest, but also suggests that upon PvHcT-treatment, *F. oxysporum* spores become unable to repair damaged membranes. The rapid degradation of peroxisomes in yeast has been associated to specific autophagy processes (pexophagy) eliminating damaged peroxisomes [61]. Peroxisomes also undergo rapid pexophagy when the metabolic pathways they contain are no longer required for cellular metabolism. However, in PvHcT-treated spores, peroxisomes may not have been produced rather than degraded. Unlike histatin-5, which has been shown to inhibit respiration [62] after translocation into the cytoplasm in a non-lytic manner [52] or through an energy-dependent local membrane disruption process [63], we did not observe any specific effect of PvHcT-treatment on mitochondria. Unlike some antifungal plant defensins [22], PvHcT did not induce signs of apoptosis in hyphae neither.

4.5. Mechanism of antifungal activity of PvHcT

Altogether our structural and biological data strongly suggest that PvHcT antifungal activity is a direct consequence of its membrane-activity. Indeed, we showed (i) that PvHcT has an α -helical amphipathic structure compatible with insertion into biological membranes, (ii) it creates membrane damages of limited size in fungal membranes, and (iii) it permeabilizes fungal membranes at doses consistent with its MIC. Consistent with its absence of antibacterial activity [19], we also found that PvHcT fails to permeabilize membranes of bacteria. We believe that this ability to specifically permeabilize fungal but not bacterial membranes is responsible for its specificity of action against fungi. Interestingly, we found that PvHcT was unable to acquire its α -helical structure in fully anionic SDS micelles, but in DPC micelles which mimic phosphatidylcholine zwitterionic membranes. This is consistent with fungal membrane composition, and especially *F. oxysporum* one, which contains zwitterionic phospholipids as major components (about 70-80% PC/PE) together with a lower and variable proportion of anionic phospholipids (essentially PS) [35].

PvHcT was also unable to permeabilize PC liposomes containing ergosterol. This indicates that the mechanism of its antifungal activity does not involve a particular interaction with the sterol of fungal plasma membrane. The capacity of antifungals to permeabilize liposomes can depend on the charge and unsaturation of lipids [64]. Therefore the lack of PvHcT activity on model membranes could result from the use of PC as the only lipid. Alternatively, insertion of PvHcT into membranes could require a membrane potential, which is lacking in the liposomes used. Such an energy-dependent mechanism of action has been found to be critical for other membrane-active peptides [65]. Finally, another likely hypothesis is that like for histatin-5 or NaD1 [52,53], a specific receptor/docking molecule present at the fungal cell wall or membrane could be required for PvHcT recognition, concentration and further insertion into the fungal membrane.

In conclusion, we have characterized here the structure and mechanism of action of an antifungal peptide involved in crustacean immunity. One interesting feature of PvHcT is that it is encoded in the most abundant plasma protein of crustaceans, the hemocyanin. Therefore, unlike gene-encoded cationic defense peptides (penaeidins, crustins, ALFs...), it can be obtained in large quantities in the absence of recombinant production/purification system, by proteolytic cleavage of hemocyanin. Alternatively, it can be obtained easily by chemical synthesis as done in this article. From its marine origin and its low acidic pI, PvHcT retains antimicrobial activity in the presence of salts, while many cationic AMPs do not. Altogether, these findings open the way to new prospects on the use of marine AMPs, easy and inexpensive to produce for biomedical or agriculture/aquaculture applications.

Acknowledgements

Work carried out in Paris was supported by fundings from the National Museum of Natural History and the CNRS, and work based in Montpellier was funded by Ifremer and the CNRS. We are pleased to thank Dr. Guillaume Charrière and the Montpellier RIO Imaging platform for precious help in fluorescence microscopy experiments. We are grateful to M. Vandervennet and G. Gastine for technical assistance in microbiology. We also thank the Analytical Platform of the National Museum of Natural History for access to the NMR, mass spectrometry and transmission electronic microscopy facilities.

Conflict of interest

We declare no conflict of interest

Author contributions

SR and DDG have contributed equally to this work. They designed and managed the overall project. EB and JP helped design the study. VWP and AB performed NMR measurements and molecular modelling. VWP performed CD experiments. JLR performed fluorescence microscopy experiments. CG purified the peptides and acquired the liposome permeabilization data. VWP, JD and CD acquired the electron microscopy data. SR and DDG wrote the manuscript with help of the other authors.

References

- [1] P. Bulet, R. Stocklin, L. Menin, Anti-microbial peptides: from invertebrates to vertebrates, *Immunol Rev* 198 (2004) 169-184.
- [2] O.E. Sorensen, N. Borregaard, A.M. Cole, Antimicrobial peptides in innate immune responses, *Contrib Microbiol* 15 (2008) 61-77.
- [3] K.A. Brogden, Antimicrobial peptides: pore formers or metabolic inhibitors in bacteria?, *Nat Rev Microbiol* 3 (2005) 238-250.
- [4] M. Wilmes, B.P. Cammue, H.G. Sahl, K. Thevissen, Antibiotic activities of host defense peptides: more to it than lipid bilayer perturbation, *Nat Prod Rep* 28 (2011) 1350-1358.
- [5] R.D. Rosa, M.A. Barracco, Antimicrobial peptides in crustaceans., *Invertebrate Survival Journal* 7 (2010) 262-284.
- [6] P. Schmitt, R.D. Rosa, M. Duperthuy, J. de Lorgeril, E. Bachere, D. Destoumieux-Garzon, The Antimicrobial Defense of the Pacific Oyster, *Crassostrea gigas*. How Diversity may Compensate for Scarcity in the Regulation of Resident/Pathogenic Microflora, *Front Microbiol* 3 (2012) 160.
- [7] T.W. Flegel, Historic emergence, impact and current status of shrimp pathogens in Asia, *J Invertebr Pathol* 110 (2012) 166-173.
- [8] D.V. Lightner, R.M. Redman, C.R. Pantoja, K.F. Tang, B.L. Noble, P. Schofield, L.L. Mohney, L.M. Nunan, S.A. Navarro, Historic emergence, impact and current status of shrimp pathogens in the Americas, *J Invertebr Pathol* 110 (2012) 174-183.
- [9] D.V. Lightner, Fungus (*Fusarium*) Disease of juvenile and adult penaeid shrimp., in: D.V.L. C.J. Sindermann (Ed.), *Disease Diagnosis and Control in North American Marine Aquaculture, Developments in Aquaculture and Fisheries Science*, Elsevier. Amsterdam (Netherlands) 1988, pp. 64–69.
- [10] D. Destoumieux, P. Bulet, D. Loew, A. Van Dorsselaer, J. Rodriguez, E. Bachere, Penaeidins, a new family of antimicrobial peptides isolated from the shrimp *Penaeus vannamei* (Decapoda), *J Biol Chem* 272 (1997) 28398-28406.
- [11] D. Destoumieux, P. Bulet, J.M. Strub, A. Van Dorsselaer, E. Bachere, Recombinant expression and range of activity of penaeidins, antimicrobial peptides from penaeid shrimp, *Eur J Biochem* 266 (1999) 335-346.
- [12] D. Destoumieux, M. Munoz, C. Cosseau, J. Rodriguez, P. Bulet, M. Comps, E. Bachere, Penaeidins, antimicrobial peptides with chitin-binding activity, are produced and stored in shrimp granulocytes and released after microbial challenge, *J Cell Sci* 113 (Pt 3) (2000) 461-469.

- [13] R.D. Rosa, A. Vergnes, J. de Lorgeril, P. Goncalves, L.M. Perazzolo, L. Saune, B. Romestand, J. Fievet, Y. Gueguen, E. Bachere, D. Destoumieux-Garzon, Functional divergence in shrimp anti-lipoplysaccharide factors (ALFs): from recognition of cell wall components to antimicrobial activity, *PLoS One* 8 (2013) e67937.
- [14] E. de la Vega, N.A. O'Leary, J.E. Shockey, J. Robalino, C. Payne, C.L. Browdy, G.W. Warr, P.S. Gross, Anti-lipoplysaccharide factor in *Litopenaeus vannamei* (LvALF): a broad spectrum antimicrobial peptide essential for shrimp immunity against bacterial and fungal infection, *Mol Immunol* 45 (2008) 1916-1925.
- [15] S. Tharntada, S. Ponprateep, K. Somboonwiwat, H. Liu, I. Soderhall, K. Soderhall, A. Tassanakajon, Role of anti-lipoplysaccharide factor from the black tiger shrimp, *Penaeus monodon*, in protection from white spot syndrome virus infection, *J Gen Virol* 90 (2009) 1491-1498.
- [16] Y. Yang, H. Boze, P. Chemardin, A. Padilla, G. Moulin, A. Tassanakajon, M. Pugnieri, F. Roquet, D. Destoumieux-Garzon, Y. Gueguen, E. Bachere, A. Aumelas, NMR structure of rALF-Pm3, an anti-lipoplysaccharide factor from shrimp: model of the possible lipid A-binding site, *Biopolymers* 91 (2009) 207-220.
- [17] Y. Yang, J. Poncet, J. Garnier, C. Zatylny, E. Bachere, A. Aumelas, Solution structure of the recombinant penaeidin-3, a shrimp antimicrobial peptide, *J Biol Chem* 278 (2003) 36859-36867.
- [18] J.L. Rolland, M. Abdelouahab, J. Dupont, F. Lefevre, E. Bachere, B. Romestand, Stylicins, a new family of antimicrobial peptides from the Pacific blue shrimp *Litopenaeus stylirostris*, *Mol Immunol* 47 (2010) 1269-1277.
- [19] D. Destoumieux-Garzon, D. Saulnier, J. Garnier, C. Jouffrey, P. Bulet, E. Bachere, Crustacean immunity. Antifungal peptides are generated from the C terminus of shrimp hemocyanin in response to microbial challenge, *J Biol Chem* 276 (2001) 47070-47077.
- [20] F. Harris, S.R. Dennison, D.A. Phoenix, Anionic antimicrobial peptides from eukaryotic organisms, *Curr Protein Pept Sci* 10 (2009) 585-606.
- [21] S.Y. Lee, B.L. Lee, K. Soderhall, Processing of an antibacterial peptide from hemocyanin of the freshwater crayfish *Pacifastacus leniusculus*, *J Biol Chem* 278 (2003) 7927-7933.
- [22] K. Vriens, B.P. Cammue, K. Thevissen, Antifungal plant defensins: mechanisms of action and production, *Molecules* 19 (2014) 12280-12303.
- [23] Y.H. Chen, J.T. Yang, K.H. Chau, Determination of the helix and beta form of proteins in aqueous solution by circular dichroism, *Biochemistry* 13 (1974) 3350-3359.
- [24] K. Wuthrich, M. Billeter, W. Braun, Pseudo-structures for the 20 common amino acids for use in studies of protein conformations by measurements of intramolecular proton-proton distance constraints with nuclear magnetic resonance, *J Mol Biol* 169 (1983) 949-961.
- [25] A.T. Brünger, X-PLOR, version 3.1. A system for X-Ray Crystallography and NMR. , Yale University Press. New Haven, CT, USA. (1992).
- [26] M. Nilges, A.M. Gronenborn, A.T. Brünger, G.M. Clore, Determination of three-dimensional structures of proteins by simulated annealing with interproton distance restraints. Application to crambin, potato carboxypeptidase inhibitor and barley serine proteinase inhibitor 2. , *Protein Eng* 2 (1988) 27-38.
- [27] B.R. Brooks, R.E. Bruccoleri, B.D. Olafson, D.J. States, S. Swaminathan, M. Karplus, CHARMM: a program for macromolecular energy minimization and dynamics calculation. , *J Comput Chem* 4 (1983) 187-217.
- [28] R. Koradi, M. Billeter, K. Wuthrich, MOLMOL: a program for display and analysis of macromolecular structures. , *J Mol Graph* 14 (1996) 51-55, 29-32.
- [29] R.A. Laskowski, J.A. Rullmann, M.W. MacArthur, R. Kaptein, J.M. Thornton, AQUA and PROCHECK-NMR: programs for checking the quality of protein structures solved by NMR. , *J Biomol NMR* 8 (1996) 477-486.
- [30] K. Thevissen, F.R. Terras, W.F. Broekaert, Permeabilization of fungal membranes by plant defensins inhibits fungal growth, *Appl Environ Microbiol* 65 (1999) 5451-5458.
- [31] N.L. van der Weerden, F.T. Lay, M.A. Anderson, The plant defensin, NaD1, enters the cytoplasm of *Fusarium oxysporum* hyphae, *J Biol Chem* 283 (2008) 14445-14452.

- [32] C. Goulard, S. Hlimi, S. Rebuffat, B. Bodo, Trichorzins HA and MA, antibiotic peptides from *Trichoderma harzianum*. I. Fermentation, isolation and biological properties, *J Antibiot (Tokyo)* 48 (1995) 1248-1253.
- [33] M. Munoz, F. Vandenbulcke, J. Garnier, Y. Gueguen, P. Bulet, D. Saulnier, E. Bachere, Involvement of penaeidins in defense reactions of the shrimp *Litopenaeus stylirostris* to a pathogenic vibrio, *Cell Mol Life Sci* 61 (2004) 961-972.
- [34] P. Damberg, J. Jarvet, A. Graslund, Micellar systems as solvents in peptide and protein structure determination. , *Methods Enzymol* 339 (2001) 271-285.
- [35] T. Theis, U. Stahl, Antifungal proteins: targets, mechanisms and prospective applications. , *Cell Mol Life Sci* 61 (2004) 437-455.
- [36] D.S. Wishart, C.G. Bigam, A. Holm, R.S. Hodges, B.D. Sykes, ¹H, ¹³C and ¹⁵N random coil NMR chemical shifts of the common amino acids. I. Investigations of nearest-neighbor effects. . *J Biomol NMR* 5 (1995) 67-81.
- [37] D.K. Chang, W.J. Chien, S.F. Cheng, S.T. Chen, NMR and circular dichroism studies on the conformation of a 44-mer peptide from a CD4-binding domain of human immunodeficiency virus envelope glycoprotein, *J Pept Res* 49 (1997) 432-443.
- [38] S.C. Li, N.K. Goto, K.A. Williams, C.M. Deber, Alpha-helical, but not beta-sheet, propensity of proline is determined by peptide environment, *Proc Natl Acad Sci U S A* 93 (1996) 6676-6681.
- [39] G. van den Bogaart, J.V. Guzman, J.T. Mika, B. Poolman, On the mechanism of pore formation by melittin., *J Biol Chem* 283 (2008) 33854-33857.
- [40] S. Campagna, N. Saint, G. Molle, A. Aumelas, Structure and mechanism of action of the antimicrobial peptide piscidin, *Biochemistry* 46 (2007) 1771-1778.
- [41] X. Lauth, H. Shike, J.C. Burns, M.E. Westerman, V.E. Ostland, J.M. Carlberg, J.C. Van Olst, V. Nizet, S.W. Taylor, C. Shimizu, P. Bulet, Discovery and characterization of two isoforms of moronecidin, a novel antimicrobial peptide from hybrid striped bass, *J Biol Chem* 277 (2002) 5030-5039.
- [42] I.H. Lee, C. Zhao, Y. Cho, S.S. Harwig, E.L. Cooper, R.I. Lehrer, Clavanins, alpha-helical antimicrobial peptides from tunicate hemocytes, *FEBS Lett* 400 (1997) 158-162.
- [43] F.G. Oppenheim, T. Xu, F.M. McMillian, S.M. Levitz, R.D. Diamond, G.D. Offner, R.F. Troxler, Histatins, a novel family of histidine-rich proteins in human parotid secretion. Isolation, characterization, primary structure, and fungistatic effects on *Candida albicans*, *J Biol Chem* 263 (1988) 7472-7477.
- [44] P.A. Raj, E. Marcus, D.K. Sukumaran, Structure of human salivary histatin 5 in aqueous and nonaqueous solutions, *Biopolymers* 45 (1998) 51-67.
- [45] K. Yu, K. Park, S.W. Kang, S.Y. Shin, K.S. Hahm, Y. Kim, Solution structure of a cathelicidin-derived antimicrobial peptide, CRAMP as determined by NMR spectroscopy, *J Pept Res* 60 (2002) 1-9.
- [46] E. Vignal, A. Chavanieu, P. Roch, L. Chiche, G. Grassy, B. Calas, A. Aumelas, Solution structure of the antimicrobial peptide ranalexin and a study of its interaction with perdeuterated dodecylphosphocholine micelles, *Eur J Biochem* 253 (1998) 221-228.
- [47] B. Bechinger, M. Zasloff, S.J. Opella, Structure and orientation of the antibiotic peptide magainin in membranes by solid-state nuclear magnetic resonance spectroscopy, *Protein Sci* 2 (1993) 2077-2084.
- [48] R.T. Syvitski, I. Burton, N.R. Mattatall, S.E. Douglas, D.L. Jakeman, Structural characterization of the antimicrobial peptide pleurocidin from winter flounder, *Biochemistry* 44 (2005) 7282-7293.
- [49] S.A. Lee, Y.K. Kim, S.S. Lim, W.L. Zhu, H. Ko, S.Y. Shin, K.S. Hahm, Y. Kim, Solution structure and cell selectivity of piscidin 1 and its analogues, *Biochemistry* 46 (2007) 3653-3663.
- [50] E.J. van Kan, A. van der Bent, R.A. Demel, B. de Kruijff, Membrane activity of the peptide antibiotic clavanin and the importance of its glycine residues, *Biochemistry* 40 (2001) 6398-6405.
- [51] G. Wang, Structures of human host defense cathelicidin LL-37 and its smallest antimicrobial peptide KR-12 in lipid micelles, *J Biol Chem* 283 (2008) 32637-32643.
- [52] X.S. Li, M.S. Reddy, D. Baev, M. Edgerton, *Candida albicans* Ssa1/2p is the cell envelope binding protein for human salivary histatin 5, *J Biol Chem* 278 (2003) 28553-28561.

- [53] N.L. van der Weerden, R.E. Hancock, M.A. Anderson, Permeabilization of fungal hyphae by the plant defensin NaD1 occurs through a cell wall-dependent process, *J Biol Chem* 285 (2010) 37513-37520.
- [54] G.S. Chitarra, P. Breeuwer, F.M. Rombouts, T. Abee, J. Dijksterhuis, Differentiation inside multicelled macroconidia of *Fusarium culmorum* during early germination, *Fungal Genet Biol* 42 (2005) 694-703.
- [55] M.R. Bleackley, J.L. Wiltshire, F. Perrine-Walker, S. Vasa, R.L. Burns, N.L. van der Weerden, M.A. Anderson, Agp2p, the plasma membrane transregulator of polyamine uptake, regulates the antifungal activities of the plant defensin NaD1 and other cationic peptides, *Antimicrob Agents Chemother* 58 (2014) 2688-2698.
- [56] H. Choi, D.G. Lee, Antifungal activity and pore-forming mechanism of astacidin 1 against *Candida albicans*, *Biochimie* 105 (2014) 58-63.
- [57] J.M. Nascimento, M.D. Oliveira, O.L. Franco, L. Migliolo, C.P. de Melo, C.A. Andrade, Elucidation of mechanisms of interaction of a multifunctional peptide Pa-MAP with lipid membranes, *Biochim Biophys Acta* 1838 (2014) 2899-2909.
- [58] H. Sato, J.B. Feix, Peptide-membrane interactions and mechanisms of membrane destruction by amphipathic α -helical antimicrobial peptides. , *Biochim Biophys Acta* 1758 (2006) 1245-1256.
- [59] Z. Kang, L. Huang, U. Krieg, A. Mauler-Machnik, H. Buchenauer, Effects of tebuconazole on morphology, structure, cell wall components and trichothecene production of *Fusarium culmorum* in vitro, *Pest Manag Sci* 57 (2001) 491-500.
- [60] R.J. Wanders, J.M. Tager, Lipid metabolism in peroxisomes in relation to human disease, *Mol Aspects Med* 19 (1998) 69-154.
- [61] T. van Zutphen, M. Veenhuis, I.J. van der Klei, Damaged peroxisomes are subject to rapid autophagic degradation in the yeast *Hansenula polymorpha*, *Autophagy* 7 (2011) 863-872.
- [62] E.J. Helmerhorst, P. Breeuwer, W. van't Hof, E. Walgreen-Weterings, L.C. Oomen, E.C. Veerman, A.V. Amerongen, T. Abee, The cellular target of histatin 5 on *Candida albicans* is the energized mitochondrion, *J Biol Chem* 274 (1999) 7286-7291.
- [63] A.B. Mochon, H. Liu, The antimicrobial peptide histatin-5 causes a spatially restricted disruption on the *Candida albicans* surface, allowing rapid entry of the peptide into the cytoplasm, *PLoS Pathog* 4 (2008) e1000190.
- [64] J. Palma-Guerrero, J.A. Lopez-Jimenez, A.J. Perez-Berna, I.C. Huang, H.B. Jansson, J. Salinas, J. Villalain, N.D. Read, L.V. Lopez-Llorca, Membrane fluidity determines sensitivity of filamentous fungi to chitosan, *Mol Microbiol* 75 (2010) 1021-1032.
- [65] D. Destoumieux-Garzon, X. Thomas, M. Santamaria, C. Goulard, M. Barthelemy, B. Boscher, Y. Bessin, G. Molle, A.M. Pons, L. Letellier, J. Peduzzi, S. Rebuffat, Microcin E492 antibacterial activity: evidence for a TonB-dependent inner membrane permeabilization on *Escherichia coli*, *Mol Microbiol* 49 (2003) 1031-1041.

Table 1. Structural statistics for the NMR solution structures of PvHct and Ace-PvHct-NH₂ in the presence of DPC micelles and in methanol solution, respectively.

	PvHct	Ace-PvHct-NH ₂
Energetic parameters (kcal.mol ⁻¹) ^a		
Bond	10.4 ± 0.35	11.62 ± 0.36
Angle	49.24 ± 3.45	40.77 ± 3.29
Dihedral	82.99 ± 4.68	84.87 ± 3.83
Improper	0.78 ± 0.14	0.67 ± 0.17
van der Waals	-44.24 ± 5.40	-57.36 ± 6.34
Electrostatic	0.9 ± 0.23	-1.24 ± 0.84
NOE restraint ^b	6.8 ± 1.23	1.16 ± 0.31
Dihedral restraint ^c	-	0.0
Total energy	106.9 ± 7.34	80.51 ± 8.19
Deviations from ideal geometry		
RMSD bond (Å)	0.009	0.01
RMSD angle (°)	2.17 ± 0.08	1.95 ± 0.08
RMSD improper (°)	1.24 ± 0.16	0.97 ± 0.23
Ramachandran (%)		
Most favored	72.5	78.1
Additionally allowed	24.2	15.8
Generously allowed	2.2	3.9
Disallowed	1.1	2.2
Pairwise atomic RMSD (Å) ^d		
Backbone atoms	0.40 ± 0.14	0.41 ± 0.14
Heavy atoms	1.37 ± 0.37	1.30 ± 0.19

^a The parameters are from CHARMM22 ; the van der Waals energy is calculated with a switched Lennard-Jones potential and electrostatic energy with a shifted Coulomb potential with a dielectric constant $\epsilon = 80.0$ (water) or 32.7 (methanol).

^b The experimental energy was calculated with a square-well potential and with a force constant of 50 kcal mol⁻¹ Å⁻².

^c The experimental energy was calculated with a force constant of 20 kcal.mol⁻¹.rad².

^d Residues selected for the fit are 6-16 for PvHct in DPC and 8-18 for Ace-PvHct-NH₂ in CD₃OH.

Table 2. Statistics for the ultrastructure changes observed in *F. oxysporum* spores treated or not (control) with PvHct (percentages of spores including the observed structures).

	Lipid bodies	Mitochondria	Peroxisomes	Cell debris
t0 control ^a	77	17	0	10
t12 control ^a	37	0	63	18
t12 PvHct ^b	43	3	0	40

^a number of spores counted: 60

^b number of spores counted: 150

Figure legends

Fig. 1. Alignment of PvHCt peptide with C-terminal sequences derived from *L. vanamei* hemocyanin genes. Sequence names / genebank accession numbers are shown on the left. Theoretical isoelectric points (pI) are shown on the right. Residues differing from the PvHCt sequence are highlighted in gray.

Fig. 2. CD analysis of the conformational changes of PvHCt in different environments. (A) CD spectra of PvHCt in phosphate buffer at pH 7, in the absence and presence of DPC and SDS micelles, and of Ace-PvHCt-NH₂ in methanol. (B) CD spectra of PvHCt in citrate buffer at pH 3, in the absence and presence of DPC micelles, and of Ace-PvHCt-NH₂ in methanol.

Fig. 3. Three-dimensional structure of PvHCt. Superposition of backbone atoms of the 20 final NMR-derived lowest energy structures of PvHCt in interaction with DPC micelles (A) and of Ace-PvHCt-NH₂ in methanol (D), respectively (B, C, E, F). The structures include an amphiphatic α -helix spanning the central region (acidic, basic and aromatic residues are coloured red, green and black, respectively; proline is coloured blue, other residues are not shown).

Fig. 4. PvHCt binds to the surface of *F. oxysporum* hyphae. Non-treated (negative control) and PvHCt-treated hyphae were stained with anti-PvHCt antibodies (green fluorescence). Nuclei were stained with DAPI (blue fluorescence). Hyphae were observed under a fluorescence microscope (40x). PvHCt detection is observed at the surface of PvHCt-treated hyphae only.

Fig. 5. PvHCt induces membrane damages in *F. oxysporum* hyphae. Hyphae were treated with increasing concentrations of PvHCt (from 1.25 to 20 μ M) in the presence of SYTOX green. (A) Hyphae observed after 2.5 h under a fluorescence microscope (40x). Light and fluorescence pictures are merged. (B) Time-course of SYTOX green uptake monitored by fluorescence spectrometry. Each point represents the mean of three individual measurements \pm S.E.

Fig. 6. Characterization of membrane damages caused by PvHCt in *F. oxysporum*. Hyphae were treated with increasing concentrations of PvHCt (10-50 μ M) and incubated with SYTOX green, 4 kDa FITC-dextran or 10 kDa FITC-dextran and observed under a fluorescence microscope (40x). Only small fluorescent dyes (SYTOX green and 4 kDa FITC-dextran beads) stain the cytoplasm of PvHCt-treated hyphae.

Fig. 7. Transmission electron microscopy of *F. oxysporum* hyphae sections. A-D. Hyphae treated for 24 h with 50 μ M PvHCt. (A) At low magnification many ghost cells (GC, *black arrows*) are observed together with a high number of daughter hyphae (DH, *white arrows*). (B,C) The daughter hyphae cell wall (dcw) are thick compared to parent hyphae cell wall (cw). (B) Some parent hyphae have a preserved integrity of the cytoplasmic organelles. (C) Some show a retracted cytoplasm with an intact plasma membrane (mb). (D) Some have a disrupted cytoplasmic membrane and the cytoplasmic content is degraded. E-F. Control hyphae containing mitochondria (m) and lipid bodies (l) and an intact plasma membrane (mb).

Fig. 8. Transmission electron microscopy of *F. oxysporum* spore sections. A, control spore containing large lipid body (l) and an intact plasma membrane (mb) (*black arrow*); B, control spore at 12 h, showing the beginning of germination with the development of peroxisomes (p); C, a spore 12 h after PvHCt treatment showing a significant decrease of lipid bodies and a damaged plasma membrane.

Name		Cter sequence		Theoretical pI
PvHCt	1	FEDLPNFGHIQVKVFNHGEHIHH	23	6.16
AHY86474	147	FEDLPNFGHIQVKVFNHGEHIHH	169	6.16
AHY86478	358	FEDLPNFGHIHV KVFNHGEHIHH	380	6.27
CAB85965	649	FEDLPNFGHIHLKVFNHGEHIHH	671	6.27
AIN41163	649	FEDLPNFGHIQVKVFNHGVHIKQN	672	6.27
AHN85635	641	FEDLPNFKHIQVKVFNHGEHI-H	662	6.43
ADZ15149	650	FEDLPNFGHIRVKVFNHGEHIHH	672	6.54
AHY86477	654	FEDLPNFKHIQVKVFNHGEHIHH	676	6.54

Figure 1

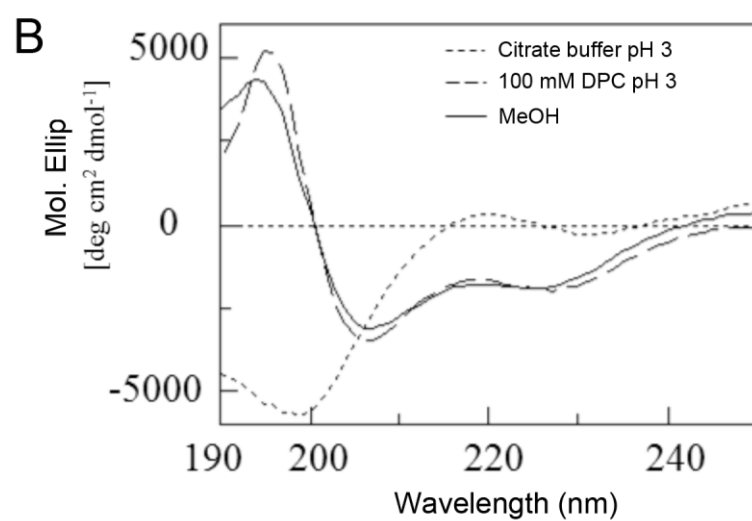
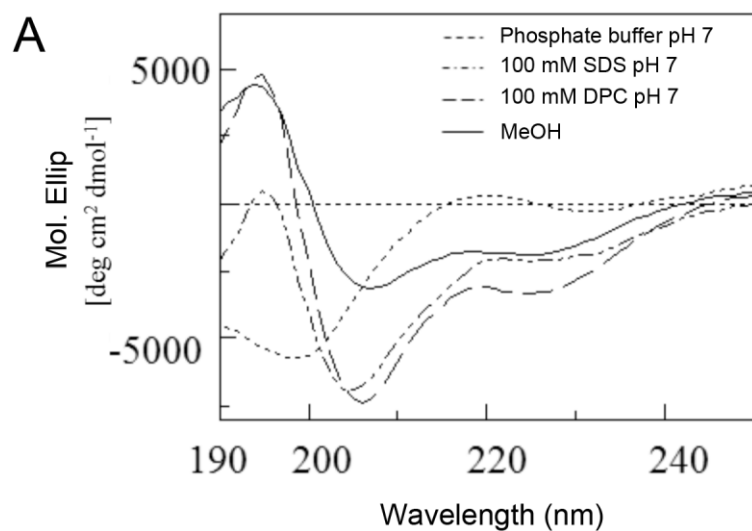


Figure 2

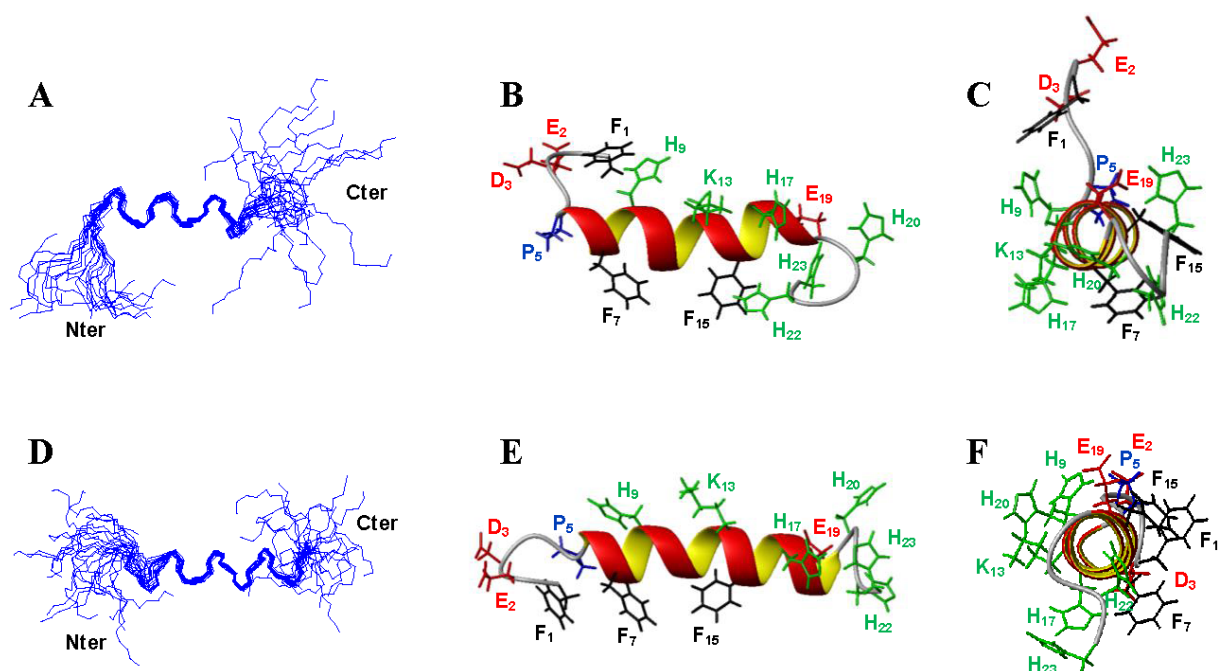
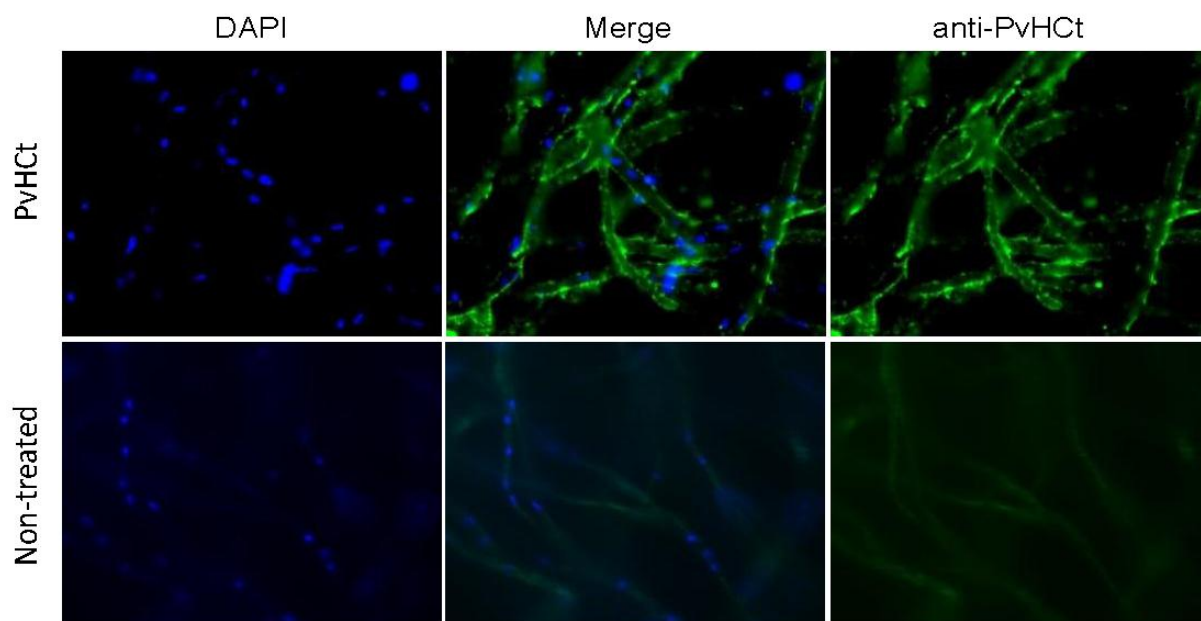


Figure 3

**Figure 4**

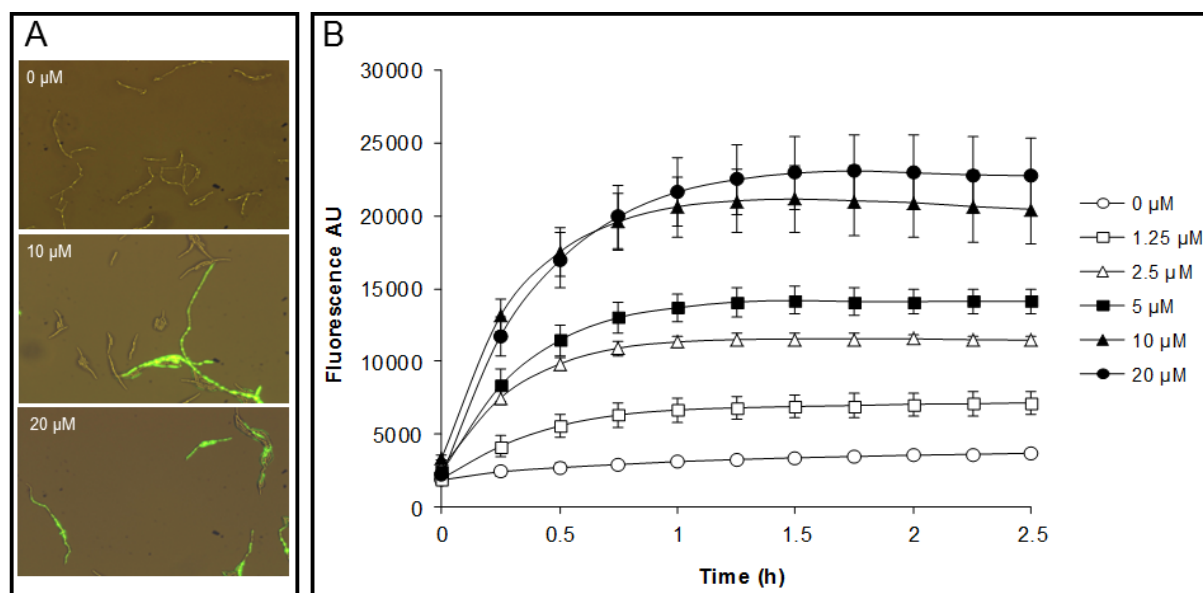
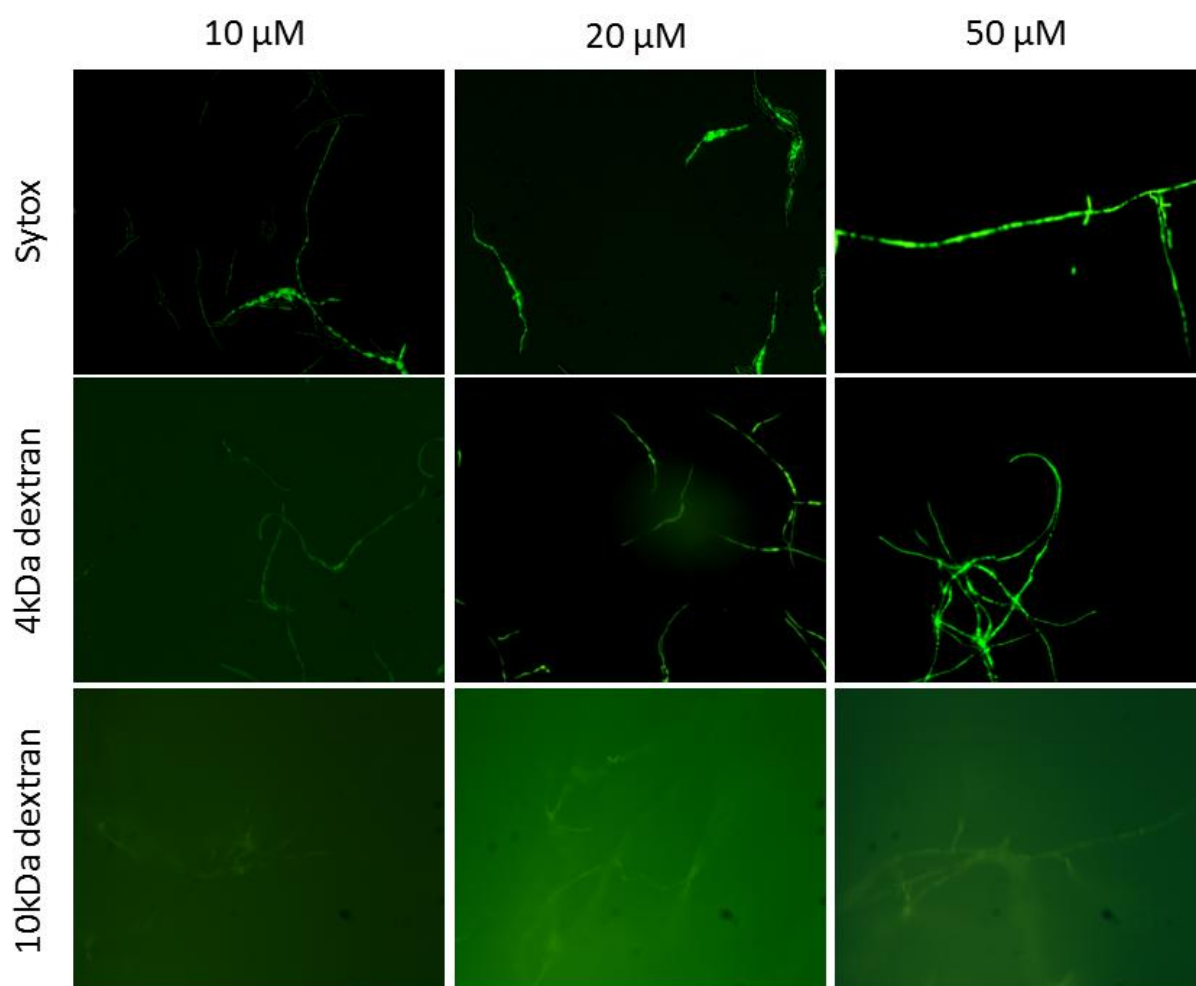


Figure 5

**Figure 6**

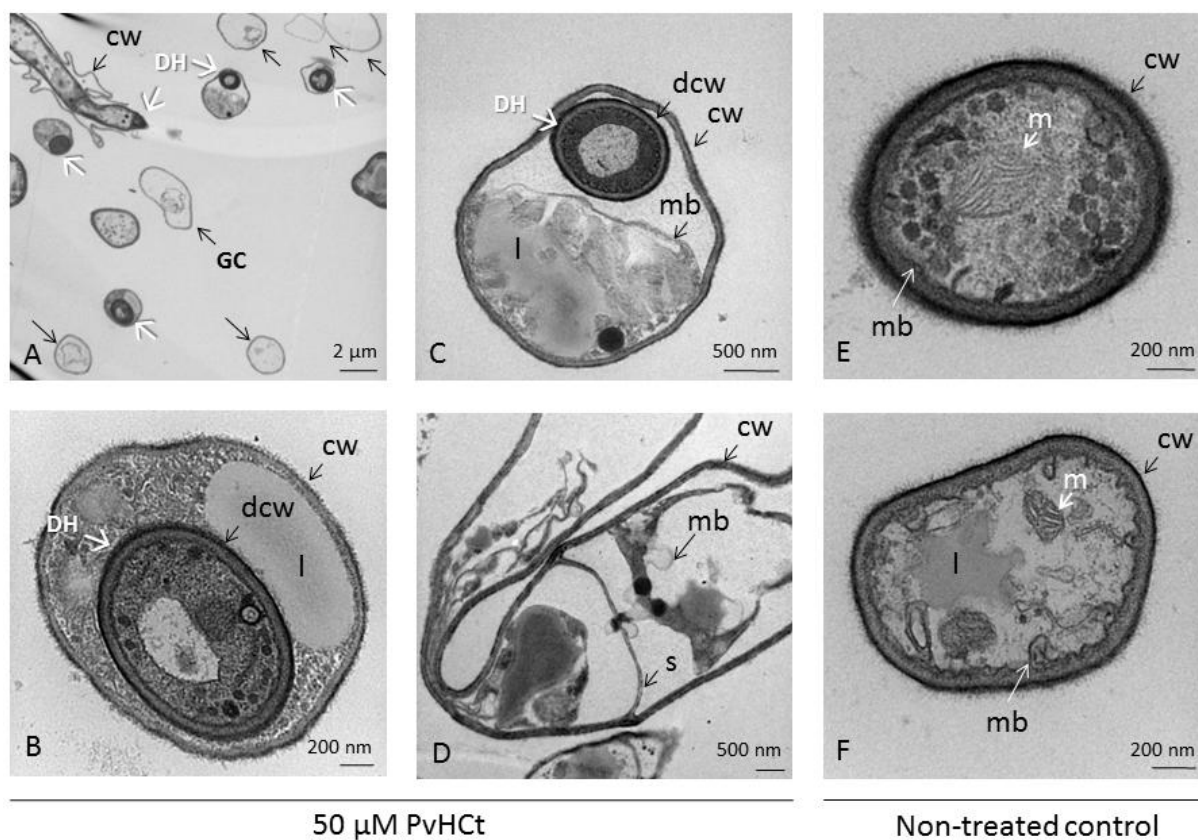
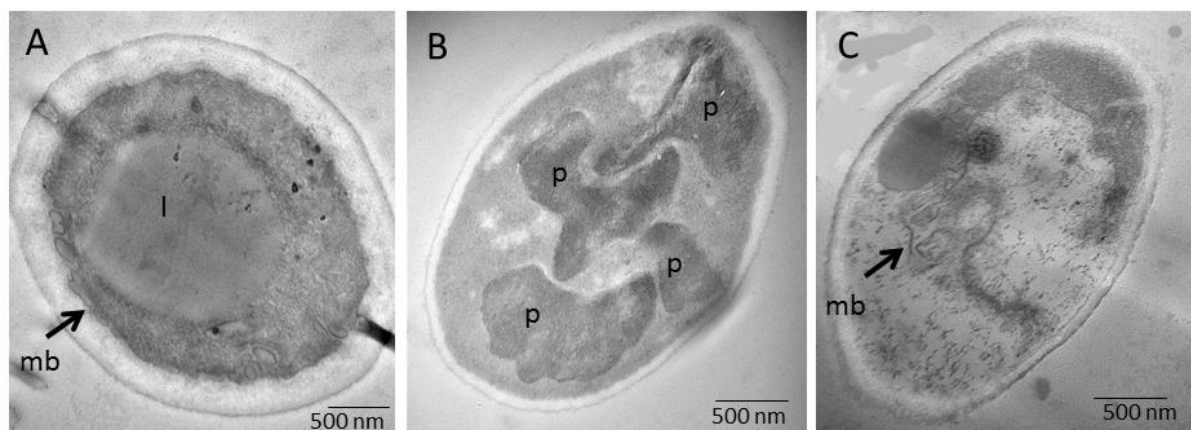
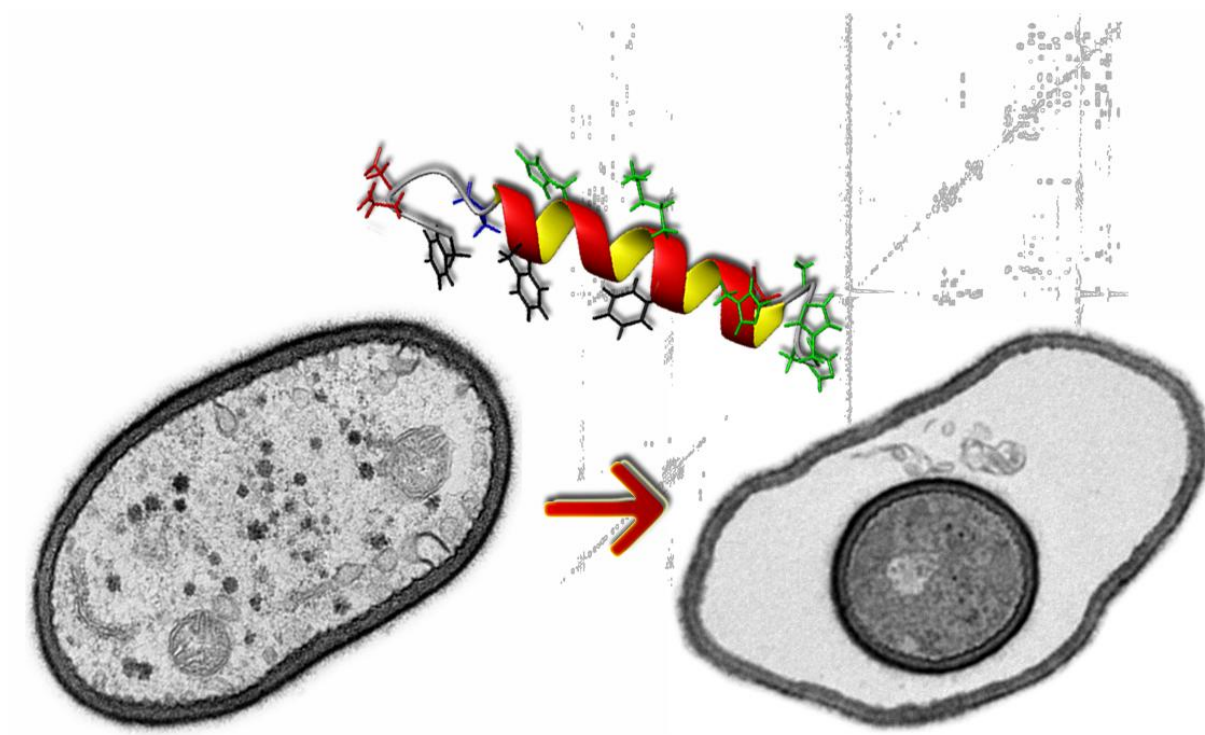


Figure 7

ACCEPTED

**Figure 8**



Graphical abstract

ACCEPTED MANUSCRIPT